Hybrid Edge Results in Narrowed Band Gap: Bottom-up Liquid-phase Synthesis of Bent N=6/8 Armchair Graphene Nanoribbons

Gang Li[1,2]†, Hanfei Wang [3]†, Michael Loes[2]†, Anshul Saxena[4], Jiangliang Yin[1], Mamun Sarker[2], Shinyoung Choi[1], Narayana Aluru*[4], Joseph W. Lyding*[3], Alexander Sinitskii*[2] and Guangbin Dong*[1]

[1]Department of Chemistry, University of Chicago, Chicago, IL 60637, USA
[2]Department of Chemistry, Nebraska Center for Materials and Nanoscience, University of Nebraska – Lincoln, Lincoln, NE 68588, USA
[3]Department of Electrical and Computer Engineering, Holonyak Micro and Nanotechnology Laboratory, University of Illinois at Urbana−Champaign, Champaign, Illinois 61801, USA
[4]Walker Department of Mechanical Engineering, Oden Institute for Computational Engineering and Sciences, The University of Texas at Austin, Austin, Texas 78712, USA
[†]These authors contributed equally to this work.

Abstract: Scalable fabrication of graphene nanoribbons with narrow band gaps has been a nontrivial challenge. Here, we have developed a unique approach to access narrow band gaps by using hybrid edge structures. Bottom-up liquid-phase synthesis of bent N=6/8 armchair graphene nanoribbons (AGNRs) has been achieved in high efficiency through copolymerization between an ortho-terphenyl monomer and a naphthalene-based monomer, followed by Scholl oxidation. An unexpected 1,2-aryl migration has been discovered, which is responsible for introducing kinked structures to the GNR backbones. The N=6/8 AGNRs have been fully characterized to support the proposed structure, which also show the narrow band gap and relatively high conductivity. In addition, their application in efficient gas sensing has also been demonstrated.

Introduction

Nanometer-wide strips of graphene, namely graphene nanoribbons (GNRs), have emerged as an attractive class of organic materials for various utilities, such as electronic, spintronic, photonic, sensing, bioimaging, quantum information processing, and energy conversion/storage devices.[1-8] Such diverse applications of GNRs benefit from their unique and versatile electronic,[4, 9-15] optical,[11, 16-17] and magnetic properties,[18-19] which are mainly dictated by the molecular structure of the ribbons. By changing their length, width, heteroatom doping, topology and edge structures or incorporating defects, the performance of GNRs can be engineered.[2, 4, 10, 20-25] Among various properties of organic semiconductors, band gap—the minimum energy required to excite an electron up to a state in the conduction band—is among one of the most important factors for device applications, which directly dictates conductivity of the materials.[26-27] While a number of atomically precise GNRs have been prepared to date, very few of them can exhibit a relative narrow band gap to allow for decent conductivity.[28-31] Hence, structurally well-defined GNRs that are stable and scalable with narrow band gaps and high processability remain highly sought after for future nanoelectronics applications.

GNRs with armchair-shaped edges, namely AGNRs, have been among the most studied GNRs from theory to date, and their band gaps are strongly correlated to the width of the ribbons.[4-5, 32-33] While AGNRs with N=3k+2 widths (N: the number of rows of atoms forming the ribbon width; k is an integer) are predicted to be semi-metallic, others (N=3k and 3k+1) are all considered to be semi-conducting materials. While ribbons with narrow band gaps have been successfully obtained with N=3k+2 or very wide AGNRs, these AGNRs are generally not trivial to prepare and often require unique monomers or special operations.[32, 34-44] In contrast, the N=3k AGNRs can be more easily accessed. For example, using an ortho-terphenyl-monomer based approach, we have efficiently prepared N=6 and 9 AGNRs through Suzuki polymerization followed by Scholl oxidation in solution.[20, 45] Given the semi-metallic feature of N=3k+2 AGNRs and the excellent accessibility of N=3k AGNRs, an intriguing question is whether the GNRs with a hybrid armchair edge, e.g., the merge between N=6 and N=8, would be easily prepared and provide a narrow band gap (Fig. 1). Stimulated by this question, here we describe the liquid-phase bottom-up scalable synthesis and characterization of N=6/8 hybrid AGNRs that indeed exhibit narrow band gaps and relatively high conductivity, as well as their use in efficient gas sensing.

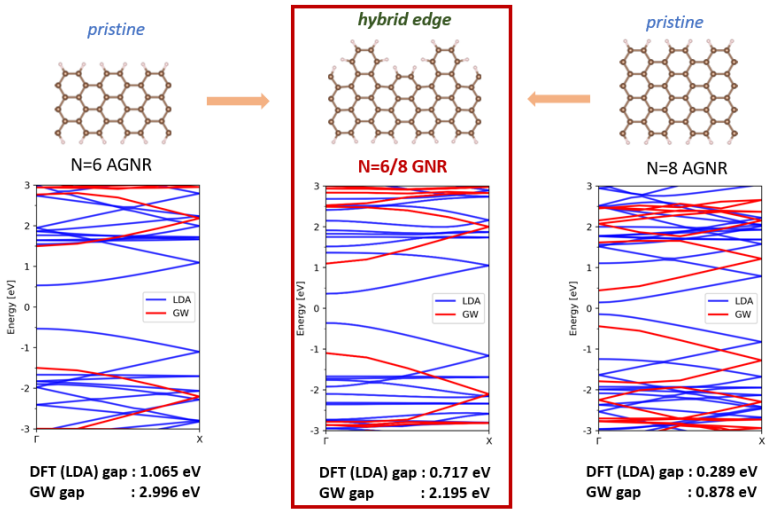

Figure 1. Comparison of the band structures of pristine N = 6 AGNR and N = 8 AGNR with the hybrid N = 6/8 AGNR.

Results and Discussion

GNR synthesis. First, our density functional theory (DFT) and first-principles calculations with GW approximation show that the proposed hybrid N=6/8 AGNR that contains alternating 6/8/6/8 armchair edges should have a band gap value in between those of N=6 and N=8 AGNRs. According to the DFT simulations, the LDA band gap of the N=6/8 AGNR is 0.717 eV, which is significantly lower than the one of the pristine N=6 AGNR (1.065 eV). The same trend can be observed with the ones obtained from first-principles calculations with GW approximation. It is noteworthy that, in the simulated structure of this new ribbon, while minor C−H bond distortion is observed in the “cove-like” regions, the whole ribbon remains its planarity (see Supporting Information), which is consistent with the predicted narrow band gap of this molecule.

Scheme 1. The Proposed Synthesis of N=6/8 AGNRs

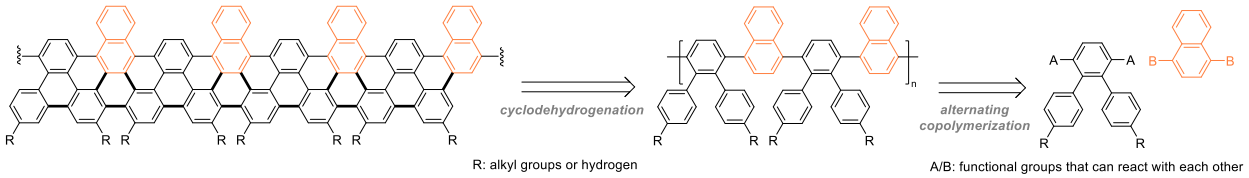

Motivated by the theoretical prediction, efforts were next made to synthesize this N=6/8 AGNR. Based on our previous work on the synthesis of N=6 AGNRs,[20] we hypothesize that the hybrid AGNR could be assembled via alternating copolymerization of an ortho-terphenyl monomer and a 1,4-naphthyl monomer (Scheme 1). To test this hypothesis, a model study on the synthesis of a structurally related nanographene (**G0'**) was first carried out (Scheme 2). The nanographene precursor **T1** was rapidly prepared in good yield from a mono-bromo-terphenyl and 1,4-naphthalenediyldiboronic acid pinacol ester (see Supporting Information for details). During the cyclodehydrogenation process, while the nanographene with N=6/8 edge can indeed be formed, an unexpected formal "alkyl transposition" was observed under the typical Scholl oxidation conditions (Scheme 2a). Both the substrate **T1** and the product **G0** were unambiguously characterized by X-ray crystallography. In this reaction, one aryl substituent on the naphthalene core migrated from the α position to the β position, and the other aryl substituent remained unmoved. *The naphthalene core is needed for this migration,* as, shown in our previous study with a simple phenylene unit in the middle,[20] no such rearrangement was observed. We propose that, the reaction is initiated by forming a benzylic cation via either the radical cation or arenium ion pathway,[46] followed by C–C bond formation with the ortho aryl group to generate a five-membered intermediate, which, after further electron-transfer, undergoes 1,2-aryl migration to give the rearranged product eventually (Scheme 2b).[47] This result indicates that, during the Scholl oxidation, aryl 1,2-migration on the naphthalene unit may compete with the direct cyclodehydrogenation, which could potentially introduce "turns" in AGNRs.

Scheme 2. An Unexpected 1,2-Aryl Migration in the Model Study

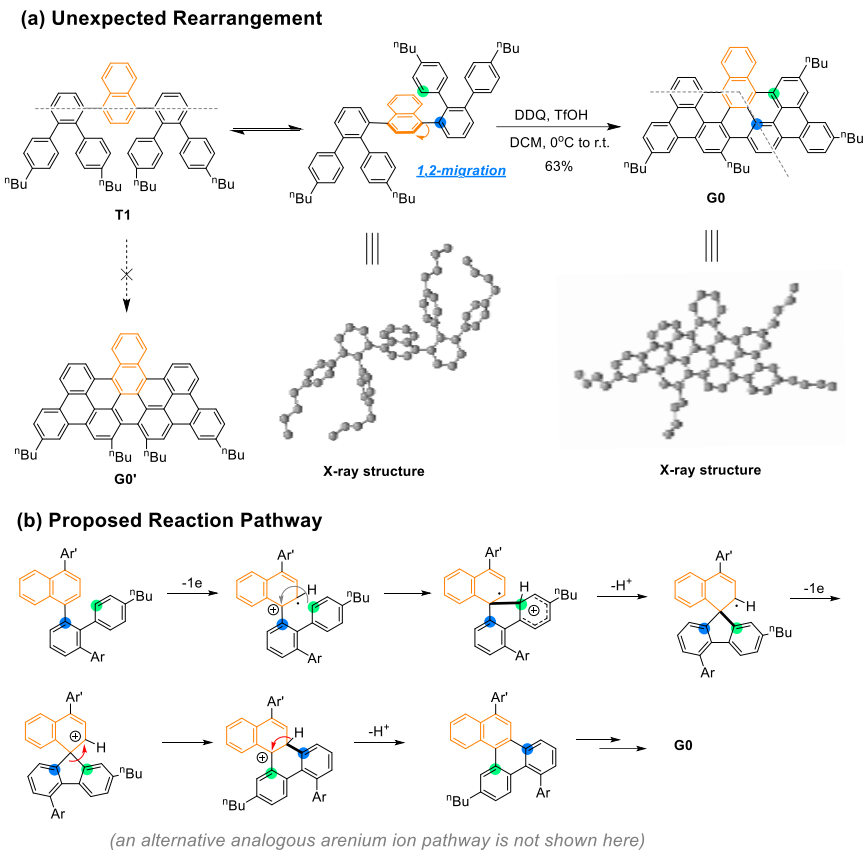

While 60° kinks could potentially be introduced to the N=6/8 GNRs according to the model study, we postulated that such 1,2-migration may not occur frequently in the actual GNR fabrication due to the more rigid C–C bonds in a polymer backbone, especially in the absence of alkyl substituents. If this defect only takes place occasionally, such bent AGNRs should still exhibit similar narrow band gaps as predicted by the theory (Scheme 3a). To examine this postulate, the Suzuki–Miyaura copolymerization of the ortho-terphenyl monomer (**M1** or **M2**) and 1,4-naphthalenediyldiboronic acid pinacol ester (**M3**) was carried out (Scheme 3b). When using $Pd(P^tBu_3)_2$ as the pre-catalyst in combination with 5 M K_3PO_4 at 50 °C, the desired GNR polymer (**P1**) was obtained in 75% yield and high molecular weight (entry 1). Interestingly, decreasing the concentration of K_3PO_4 to 3 M provided **P1** in even higher molecular weight and higher yield (entry 2). These materials were suitable for size exclusion chromatography (SEC) analysis due to their excellent solubility. The MALDI-TOF mass spectra analysis indicated that the m/z intervals are in well agreement with the exact mass of the repeating unit (634), and the end groups were phenyl groups (-Ph) for **P1** (see Fig. 2a and Supporting Information Fig. S1). The polymer precursor (**P2**) with alkyl side chains was prepared using a similar protocol in excellent yield (97%) and relatively low-molecular weight (entry 3). Soxhlet extraction of the polymer sample under refluxing acetone for 24 hours resulted in relatively high-molecular weight (Mn: 9.6 KDa, entry 3) due to the removal of low-molecular oligomers.

The final cyclodehydrogenation was carried out using the 2,3-dichloro-5,6-dicyano-1,4-benzoquinone (DDQ)/ trifluoromethanesulfonic acid (TfOH) protocol (Scheme 3c).[20] Both polymer precursors can be converted to the corresponding GNRs smoothly. After washing with water and Soxhlet extraction with boiling methanol, **G1** and **G2** were isolated as black powders.

Scheme 3. Synthesis of Bent N=6/8 AGNRs

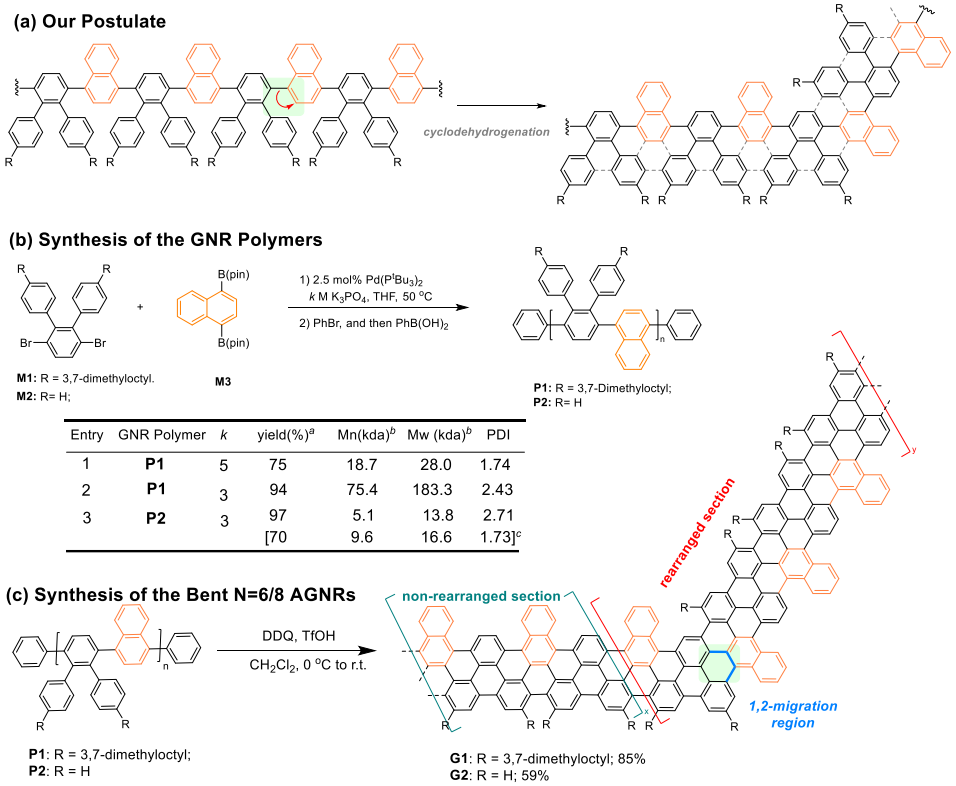

Entry	GNR Polymer	*k*	yield(%)[a]	Mn(kda)[b]	Mw (kda)[b]	PDI
1	**P1**	5	75	18.7	28.0	1.74
2	**P1**	3	94	75.4	183.3	2.43
3	**P2**	3	97	5.1	13.8	2.71
			[70	9.6	16.6	1.73][c]

[a]Isolated yield. [b]Determined by THF SEC calibrated with polystyrene standards. [c]After Soxhlet extraction under reflux of acetone. r.t., room temperature.

GNR characterization. Likely owing to their bent structures, **G1** and **G2** can be well dispersed in THF, chlorobenzene, and o-dichlorobenzene, these samples were next fully characterized by Fourier-transform infrared (FTIR), Raman, UV–Vis–NIR spectroscopy, and scanning tunning microscopy (STM).

The efficiency of the oxidative cyclodehydrogenation, which converted polymer **P1** to GNRs **G1**, was confirmed by FTIR spectroscopy. Fig. 2b demonstrates a representative FTIR region for the material before and after cyclodehydrogenation in the spectral range from 3150 to 3000 cm^{-1}. The spectrum of the polymer **P1** contains three characteristic peaks at 3063, 3046, and 3025 cm^{-1} that originate from the aromatic C–H stretching.[48-50] These peaks are expected to be strong in polymer **P1** with abundant aryl moieties but drastically diminish in intensity upon cyclodehydrogenation, which significantly reduces the number of the C-H bonds. Correspondingly, these peaks were not observed in the FTIR spectrum of GNRs **G1**, see Fig. 2b.

Raman spectroscopy is a powerful tool for the investigation of graphene and graphene-based nanomaterials.[51-52] Fig. 2c shows Raman spectra of the GNRs with (**G1**) and without (**G2**) the 3,7-dimethyloctyl side chains. Both GNRs demonstrate the high degree of graphenization, which is shown by the presence of two intense peaks at 1350 and 1590 cm^{-1} that are typically attributed to the D and G bands, respectively, in *sp*^{2} carbon materials. The high intensity of the D band in the Raman spectra of GNRs does not necessarily represent structural defects, as in two-dimensional graphene,[51-52] but is a direct result of the symmetry breaking at the edges of nanoribbons. Other features in the Raman spectra of both GNRs are a series of less intense peaks in the 2500-3250 cm^{-1} range, which include second-order bands, such as 2D, D+G, and 2G, as well as several low-intensity peaks in the 300-450 cm^{-1} range. These peaks belong to

a frequency range where the GNRs typically exhibit radial breathing-like modes (RBLMs), which represent the fundamental transverse acoustic vibrations of nanoribbons and their wavenumbers are inversely proportional to the ribbon's width.[53] Interestingly, nanoribbons with different shapes, such as straight AGNRs[21, 53-54] or chevron-family GNRs,[29] typically exhibit a single RBLM peak, so the fact that several peaks were observed in this range may indicate the presence of segments with different widths, possibly due to the formation of kinked structures.

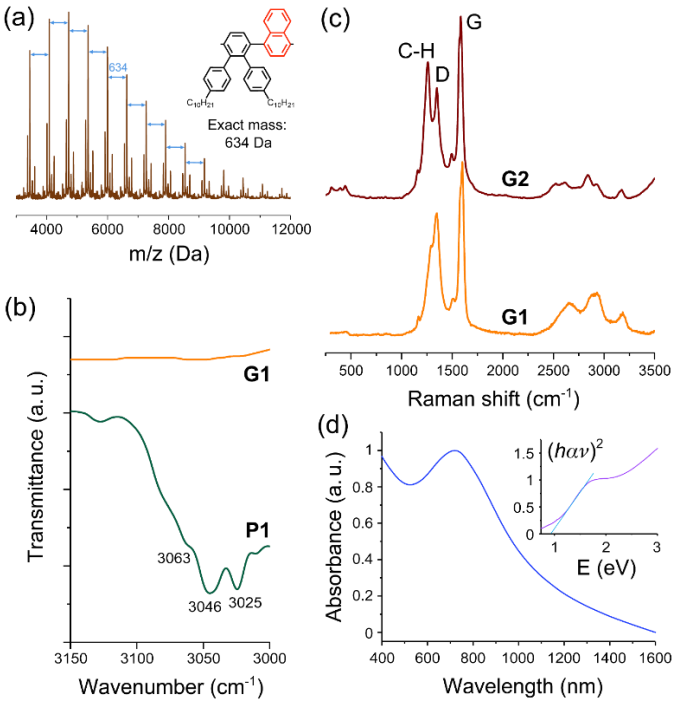

Figure 2. Characterization of the Bent N=6/8 AGNRs. (a) MALDI TOF mass spectra of **P1** (linear mode, matrix: DCTB). (b) FTIR spectra of **P1** and **G1**. (c) Raman spectra of **G1** and **G2**. (d) UV-vis-NIR optical absorption spectrum of **G1** and the corresponding Tauc plot shown in the inset.

A comparison of the two spectra in Fig. 2c demonstrates the effect of alkyl chains on the Raman signals of the N = 6/8 armchair GNR. First of all, all peaks in the spectrum of a pristine hydrogen-passivated nanoribbon (**G2**) look sharper than the same peaks in the spectrum of a functionalized GNR (**G1**) because the bulky alkyl chains dampen the atomic vibrations of the graphene lattice of a ribbon. Second, the presence of the side chains also affects the relative intensities of some of the peaks, which is particularly prominent for the pair of peaks at about 1265 and 1350 cm^{-1}, which were previously interpreted as the edge C−H and the D bands for GNRs, respectively.[55-56] In accordance with this interpretation, the C−H vibration is a prominent peak for the hydrogen-passivated **G2** nanoribbon, but the intensity of this peak decreases relative to the adjacent D band for the **G1** nanoribbon, in which some of the edge carbons are terminated with the alkyl chains instead of the hydrogen atoms.

The optical absorption spectroscopy shows that nanographene **G0** has an optical band gap of 2.46 eV, which is narrower than the corresponding pristine nanographene of N=6 AGNR (2.74 eV),[20] suggesting that the added fused benzene ring on the edge could effectively narrow the band gap (Supporting Information Fig. S2). The GNRs **G1** and **G2** exhibit broad absorption in the ultraviolet (UV), visible, and even near infrared (NIR) regions with blunt absorption onsets (Fig. 2d). Using the Tauc method,[57-58] the

optical band gap of **G1** was determined to be 1.0 eV (see the inset in Fig. 2d). The **G2** sample in THF suspension showed broad absorption with blunt absorption onset at 932 nm, which refers to an optical band gap of 1.33 eV (Supporting Information Fig. S3). The relatively wider band gap of **G2** is probably because the length of **G2** is shorter than **G1**. For comparison, when the **G2** sample was filmed on tape, an absorption onset increased to 1330 nm due to the excitonic effect from aggregation[59] of the ribbons on the tape, and the optical band gap was determined as 0.93 eV.

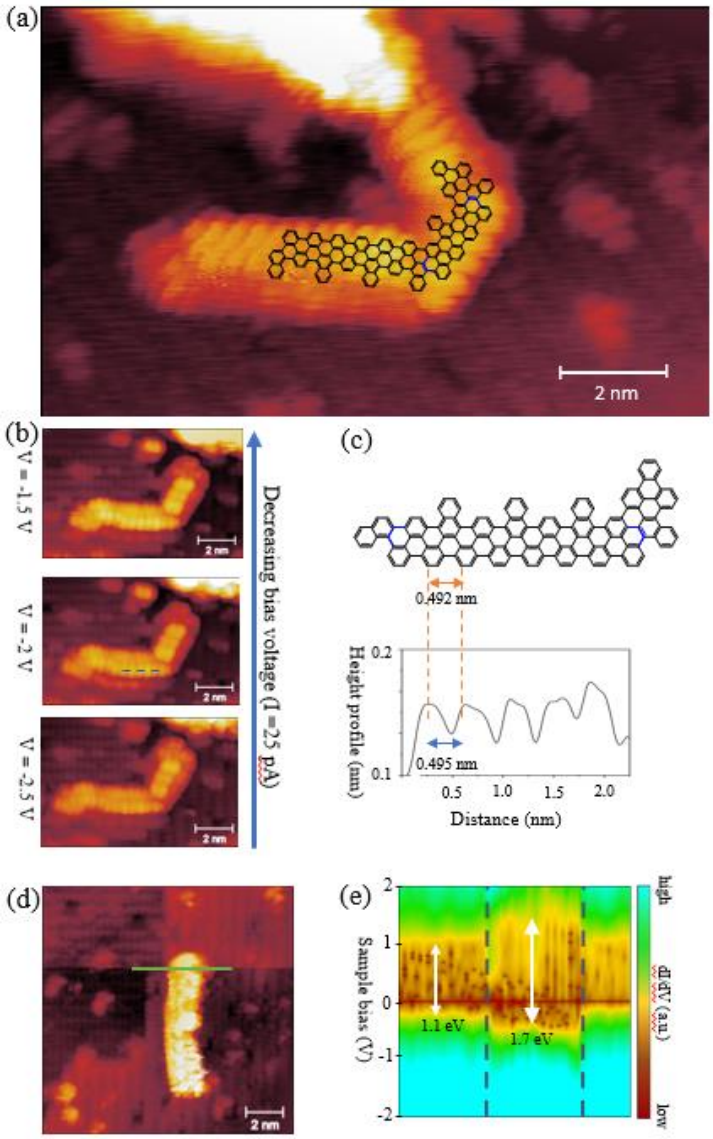

Figure 3. STM scans of G2 and topographical analysis. (a) Filled-state STM topographic images of GNR on Si(100)-2×1:H at sample bias of -1.5 V and tunneling current of 5 pA. (b) STM images of a fragment of the same ribbon taken at the same tunneling current of I = 25 pA but sample bias of V = -2.5 V, -2 V, and -1.5 V respectively. The scan length is 10.9 nm. (c) height profiles measured across the GNR from panel **b** and along its edge. The position of the height profile is indicated in panel **b** by the blue dashed line. (d) and (e) Normalized tunneling conductance spectra map along the green line across the GNR in the inset in panel **d**.

For STM characterizations, these ribbons were first transferred from ambient pressure into the ultra-high vacuum (UHV) chamber and then cleanly deposited by dry contact transfer (DCT) onto the desired target surface. Our DCT approach involves impregnating fiberglass ribbon with GNR powder in ambient pressure to make DCT applicator,[60] degassing under UHV to remove undesired contaminants, and manipulating the applicator into contact with a fresh substrate. With layered materials like graphene or GNRs, the DCT approach can effectively exfoliate the sample into monolayer or a few layers onto substrate and is minimally perturbative to both the ribbons and the substrate.[14, 61] In this study, hydrogen passivated Si surface (Si(100)-2×1:H) was used as the substrate, which has a known electronic band gap of about 1.1 eV.[62] Hydrogen passivation removes the dangling bonds of a clean silicon substrate, theoretically leaving only the van der Waals force between the substrate and the ribbons, keeping the electrical properties of the ribbons unaffected.[63] Throughout this study, we have observed that the van der Waals forces are strong enough to hold the ribbons in place for STM and scanning tunneling spectroscopy (STS) characterizations.

Topographical STM scans consistently show intriguing asymmetrical structures on the **G2** sample. Fig. 3a is a collection of filled-state STM topography taken at room temperature on the Si(100)-2×1:H substrate post DCT. The GNR fragments we found exhibit an alternating asymmetric internal structure regardless of the scanning parameters. Keeping the tunneling current constant at 25 pA and decreasing the applied voltage between the tip and the GNR surface, we gradually brought the tip apex closer to the GNR surface. When the bias voltage is at -2.5 V, the tip apex is the furthest away from the GNR surface. The imaged GNR fragment exhibits clear edge structures but no internal structures. At -1V, the tip apex is the closest to the GNR and the image exhibits more internal structure and less observable edge structure (Fig. 3b). Tunneling current is the result of the tip-sample interaction affected both by the barrier height and the electron densities of the states. The observed STM topographical images are the collection of both GNR geometric features and local density of states (LDOS). The geometric structure of the GNR fragment is invariant through different scanning parameters, and the only varying factor is the LDOS at different distances above the GNR. LDOS identifies the spatial decay of surface energy states in three dimensions. In GNRs, the LDOS of the edge structures is weaker compared to the LDOS of the internal structures but decays slower and dominates at further distance above the GNR sample. Height analysis across the internal structures of a GNR fragment is plotted in Fig. 3c. The distance between the two neighboring bright features is a close match to the small cove-like diameter in the desired N=6/8 AGNR structure. The STM topography shows, except for a few straight ones, most ribbons contain only one or two kinks in their backbones, which is consistent with our proposed structure of this AGNR.

To determine the electronic structure of this GNR, STS was next employed. The spectrum map taken across the middle of the straight GNR ribbon in Fig. 3d exhibits the STS band gap of 1.7 eV shown in Fig. 3e. As generally expected for GNRs,[64] the experimental STS band gap is smaller than the calculated GW band gap (~2.2 eV, Fig. 1) but larger than the optical band gap of about 1 eV (Fig. 2d). In comparison, for the chevron GNR, which was investigated in numerous studies, the GW band gap is about 3.8 eV,[29] its STS band gap determined for the ribbons deposited on H:Si(100), as in the present work, is about 2.8 eV,[61] and the optical band gap of about 1.6 eV, if determined using a Tauc plot.[50] In terms of the magnitude of its band gap, the N = 6/8 AGNR is comparable with the N = 9 AGNR.[65] For the latter ribbon, the calculated GW gap is 2.1 eV,[65] which is similar to that of the N = 6/8 AGNR (Fig. 1). The experimental STS band gaps of the two nanoribbons are comparable, and some difference between the reported values can be explained by the fact that 1.4 eV was found for a N = 9 AGNR that was grown and investigated on a metallic Au(111),[65] while a larger value of 1.7 eV was determined in this work for a N = 6/8 AGNR on a semiconducting silicon substrate. It was also shown for other GNRs[61, 66] that their STS measurements on semiconducting substrates provide larger band gap measurements than such measurements on Au(111); for example, the STS band gap of the chevron GNR is about 2.5 eV on Au(111)[67] and 2.8 eV on Si.[61]

GNR application in electronic devices. Because of its moderate band gap, N=9 AGNR has been a popular nanoribbon for implementation in electronic devices.[68] Since N = 6/8 AGNR has a similar band gap to N=9 AGNR, this motivated us to perform electrical characterization of the ribbons synthesized in this work. Given the previous success with the application of thin films of solution-synthesized atomically precise GNRs in gas sensors,[29, 69] we also performed electrical measurements of N = 6/8 AGNRs in a form of thin films[70] and tested their sensing response to methanol, which was used as a model analyte.

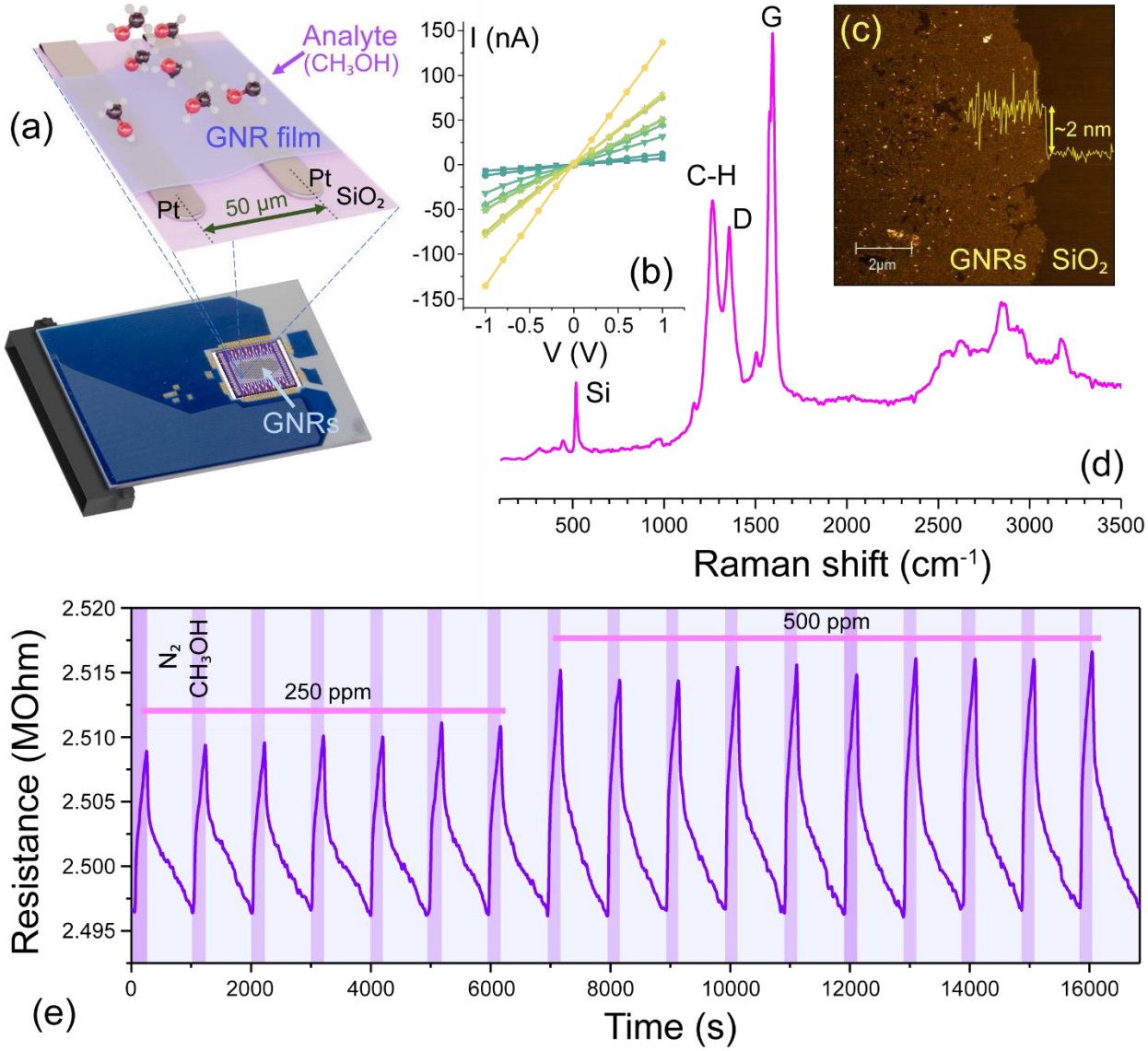

Figure 4. Application of N=6/8 AGNRs as gas sensors. (a) Schematic representation of the GNR gas sensor chip. (b) *I-V* curves for 10 segments on the sensor chip. (c) AFM image showing the edge profile of the self-assembled GNR film and a thickness of 2nm. (d) Raman spectrum of the self-assembled GNR film. (e) Representative response transients to 250 ppm and 500 ppm methanol (dark blue) compared to a N_2 baseline (light blue).

For the device fabrication, we used the **G2** sample of nonfunctionalized GNRs, because the bulky alkyl chains in the **G1** nanoribbons could affect the results of electrical measurements. The **G2** nanoribbons

were processed into thin films using the interfacial self-assembly approach developed by Shekhirev, *et al*.[70] First, a few small particles of **G2** powder (< 1 mg) were transferred to a small vial that can be capped. The powder was dissolved in chlorosulfonic acid (~1-2 mL) such that the solution appears opaque when placed on a benchtop, but when examined under illumination, a transparent solution of dark, grey-green color was observed indicating a low-bandgap semiconductor by optical absorbance. This solution was then gently dripped down a prepared glass slide into a basin of still, deionized water to form free-floating GNR films. It is known that hydrophobic GNRs self-assemble at the water-air interface in the "edge-on" geometry,[70] which minimizes their interaction with the water surface and enables the π-π stacking; this process also removes the chlorosulfonic acid from the resulting film. These self-assembled GNR films can be collected from the water surface by an arbitrary substrate. In this work, we used a p-doped silicon substrate with a 200-nm-thick layer of SiO_2 that was covered with 39 parallel Pt electrodes separated by 50 µm channels. These electrodes that form 38 device segments that can be measured independently. The sensor chip with a self-assembled GNR film bridging the Pt electrodes is schematically shown in Fig. 4a. Previously, we employed similar chips in the electronic and sensor studies of other GNRs as well as a variety of different nanomaterials, including graphene,[71] graphene oxide,[72-73] and MXenes.[74-75]

Fig. 4b shows the current (*I*) – voltage (*V*) dependences for 10 representative segments of the sensor chip covered with a self-assembled film of N = 6/8 AGNRs. The linearity of the I-V curves implies good electrical contacts between the GNR film and the Pt electrodes. Compared to the films of chevron GNRs[70] and laterally extended chevron GNRs,[29] which were fabricated by the same interfacial self-assembly approach and deposited on similar sensor chips, the N = 6/8 AGNR films were more conductive, which can be explained by their smaller band gap. Fig. 4c shows a representative atomic force microscopy (AFM) image of a self-assembled N = 6/8 AGNR film on a Si/SiO_2 substrate. Despite a few small cracks and pinholes, the film looks continuous, which enables its electrical conductivity on a scale of the 50 µm channel length. The film has a uniform thickness of about 2 nm, suggesting that this is a monolayer of GNRs arranged in the "edge-on" geometry, as discussed in our previous works.[29, 66, 70]

One of the potential issues with the interfacial self-assembly approach is the highly corrosive nature of chlorosulfonic acid.[70] In order to verify that the unfunctionalized N = 6/8 AGNRs (the **G2** sample) did not degrade in chlorosulfonic acid, we measured a Raman spectrum of the self-assembled GNR film on a Si/SiO_2 substrate (Fig. 4d). The spectrum shows the same Raman peaks as for the as-prepared **G2** sample before the chlorosulfonic acid treatment (Fig. 2c), and the peaks look narrow and sharp. A more detailed comparison of the Raman spectra of **G2** before and after the chlorosulfonic acid treatment is provided in Supporting Information Fig. S4, indicating that the N = 6/8 AGNRs did not degrade during the preparation of the sensor chip.

This sensor chip was loaded into a home-built gas sensor testing chamber[29] and exposed to mixtures of vapors in nitrogen while monitoring the electrical conductivity of each segment individually. Fig. 4e shows example response transients of a representative segment on the N = 6/8 AGNR sensor chip to repeated cycles of methanol vapor versus a nitrogen background. Immediately after fabrication the sensor behaves optimally, showing response (Response = $\frac{R_{analyte} - R_{baseline}}{R_{baseline}} * 100\%$) of a few percent for a variety of volatile organics and concentrations in the ppm range. Even after nearly 12 months in storage under ambient conditions, the sensor response remains about 1% to 500 ppm methanol, suggesting the environmental stability of N = 6/8 AGNRs in a device embodiment. In addition to stability under ambient conditions, the sensor is also stable for operation at working temperatures of at least 100 °C for prolonged experiments. As has been shown for other chemiresistive gas sensors based on semiconducting GNR films[29, 69], this operation increases both response magnitude and speed. In summary, Fig. 4 shows that,

consistent with their moderate electronic band gap, the N = 6/8 AGNRs are electrically conductive and may be promising for gas sensing applications.

Conclusion

In summary, we have demonstrated the first solution-phase fabrication of N=6/8 AGNRs that contain hybrid edges. These ribbons exhibit narrow band gaps and relatively high conductivity. This offers a new and convenient strategy to engineer band gaps using mixed edges. The discovery of the 1,2-migration during the cyclodehydrogenation has led to an interesting observation of kinked structures. DCT has been further illustrated as a powerful tool for STM characterization of insoluble GNRs. The application of these hybrid edged GNRs in efficient gas sensing could have broad implications of other innovative uses of this class of materials.

ASSOCIATED CONTENT

Supporting Information

The Supporting Information is available free of charge at

https://pubs.acs.org/doi/xx.xxxx/acsnano.xxxxxxx.

Additional experimental details, materials, methods and spectral data (PDF)

AUTHOR INFORMATION

Corresponding Author

Guangbin Dong − Department of Chemistry, University of Chicago, Chicago, IL 60637, USA;

orcid.org/0000-0003-1331-6015; Email: gbdong@uchicago.edu

Alexander Sinitskii − Department of Chemistry, University of Nebraska-Lincoln, Lincoln, NE 68588, USA;

orcid.org/0000-0002-8688-3451; Email: sinitskii@unl.edu

Joseph Lyding – Department of Engineering, University of Illinois at Urbana-Champaign, Champaign, IL 61801, USA; orcie.org/0000-0001-7285-4310; Email: lyding@illinois.edu

Narayana R. Aluru – Walker Department of Mechanical Engineering, Oden Institute for Computational Engineering and Sciences, The University of Texas at Austin, Austin, Texas 78712, USA; orcid.org/0000-0002-9622-7837; Email: aluru@utexas.edu

Authors

Gang Li − Department of Chemistry, University of Chicago, Chicago, IL 60637, USA; – Department of Chemistry, University of Nebraska-Lincoln, Lincoln, NE 68588, USA; orcid.org/0000-0001-5295-7769

Michael J. Loes – Department of Chemistry, University of Nebraska-Lincoln, Lincoln, NE 68588, USA; orcid.org/0000-0002-7743-1496

Mamun Sarker – Department of Chemistry, University of Nebraska-Lincoln, Lincoln, NE 68588, USA; orcid.org/0000-0002-1541-7066

Jiangliang Yin − Department of Chemistry, University of Chicago, Chicago, IL 60637, USA

Shinyoung Choi − Department of Chemistry, University of Chicago, Chicago, IL 60637, USA

Hanfei Wang – Department of Engineering, University of Illinois at Urbana-Champaign, Champaign, IL 61801, USA

Anshul Saxena – Walker Department of Mechanical Engineering, Oden Institute for Computational Engineering and Sciences, The University of Texas at Austin, Austin, Texas 78712, USA; orcid.org/0000-0003-4413-5030; Email: saxenaanshul@utexas.edu

Notes

The authors declare no competing financial interest.

ACKNOWLEDGMENTS

This research was supported by the National Science Foundation CHE 2002912 (on the GNR synthesis and band gap engineering, G.D.). The Office of Naval Research MURI Program N00014-19-1-2596 is gratefully acknowledged for the support of GNR characterization, STM work, computational studies, device fabrication, and sensor measurements (A.S., N.A., J.W.L.).

REFERENCES

1. Johnson, A. P.; Sabu, C.; Swamy, N. K.; Anto, A.; Gangadharappa, H.; Pramod, K. Graphene nanoribbon: An emerging and efficient flat molecular platform for advanced biosensing. *Biosens. Bioelectron.* **2021**, *184*, 113245.

2. Narita, A.; Wang, X.-Y.; Feng, X.; Müllen, K. New advances in nanographene chemistry. *Chem. Soc. Rev.* **2015**, *44*, 6616-6643.

3. Wang, T.; Wang, Z.; Salvatierra, R. V.; McHugh, E.; Tour, J. M. Top-down synthesis of graphene nanoribbons using different sources of carbon nanotubes. *Carbon* **2020**, *158*, 615-623.

4. Yano, Y.; Mitoma, N.; Ito, H.; Itami, K. A quest for structurally uniform graphene nanoribbons: synthesis, properties, and applications. *J. Org. Chem.* **2019**, *85*, 4-33.

5. Yoon, K.-Y.; Dong, G. Liquid-phase bottom-up synthesis of graphene nanoribbons. *Mater. Chem. Front.* **2020**, *4*, 29-45.

6. Chen, Z.; Narita, A.; Müllen, K. Graphene nanoribbons: on-surface synthesis and integration into electronic devices. *Adv. Mater.* **2020**, *32*, 2001893.

7. Narita, A.; Chen, Z.; Chen, Q.; Müllen, K. Solution and on-surface synthesis of structurally defined graphene nanoribbons as a new family of semiconductors. *Chem. Sci.* **2019**, *10*, 964-975.

8. Gu, Y.; Qiu, Z.; Müllen, K. Nanographenes and graphene nanoribbons as multitalents of present and future materials science. *J. Am. Chem. Soc.* **2022**, *144*, 11499-11524.

9. Son, Y.-W.; Cohen, M. L.; Louie, S. G. Energy gaps in graphene nanoribbons. *Phys. Rev. Lett.* **2006**, *97*, 216803.

10. Houtsma, R. K.; de la Rie, J.; Stöhr, M. Atomically precise graphene nanoribbons: interplay of structural and electronic properties. *Chem. Soc. Rev.* **2021**, *50*, 6541-6568.

11. Chung, H.-C.; Chang, C.-P.; Lin, C.-Y.; Lin, M.-F. Electronic and optical properties of graphene nanoribbons in external fields. *Phys. Chem. Chem. Phys.* **2016**, *18*, 7573-7616.

12. Wu, J.; Pisula, W.; Müllen, K. Graphenes as potential material for electronics. *Chem. Rev.* **2007**, *107*, 718-747.

13. Li, X.; Wang, X.; Zhang, L.; Lee, S.; Dai, H. Chemically derived, ultrasmooth graphene nanoribbon semiconductors. *Science* **2008**, *319*, 1229-1232.

14. Ritter, K. A.; Lyding, J. W. The influence of edge structure on the electronic properties of graphene quantum dots and nanoribbons. *Nat. Mater.* **2009**, *8*, 235-242.

15. Son, Y.-W.; Cohen, M. L.; Louie, S. G. Half-metallic graphene nanoribbons. *Nature* **2006**, *444*, 347-349.

16. Prezzi, D.; Varsano, D.; Ruini, A.; Marini, A.; Molinari, E. Optical properties of graphene nanoribbons: The role of many-body effects. *Phys. Rev. B* **2008**, *77*, 041404.

17. Nair, R. R.; Blake, P.; Grigorenko, A. N.; Novoselov, K. S.; Booth, T. J.; Stauber, T.; Peres, N. M.; Geim, A. K. Fine structure constant defines visual transparency of graphene. *Science* **2008**, *320*, 1308-1308.

18. Ruffieux, P.; Wang, S.; Yang, B.; Sánchez-Sánchez, C.; Liu, J.; Dienel, T.; Talirz, L.; Shinde, P.; Pignedoli, C. A.; Passerone, D.; Dumslaff, T.; Feng, X.; Müllen, K.; Fasel, R. On-surface synthesis of graphene nanoribbons with zigzag edge topology. *Nature* **2016**, *531*, 489-492.

19. Blackwell, R. E.; Zhao, F.; Brooks, E.; Zhu, J.; Piskun, I.; Wang, S.; Delgado, A.; Lee, Y.-L.; Louie, S. G.; Fischer, F. R. Spin splitting of dopant edge state in magnetic zigzag graphene nanoribbons. *Nature* **2021**, *600*, 647-652.

20. Li, G.; Yoon, K.-Y.; Zhong, X.; Wang, J.; Zhang, R.; Guest, J. R.; Wen, J.; Zhu, X.-Y.; Dong, G. A modular synthetic approach for band-gap engineering of armchair graphene nanoribbons. *Nat. Commun.* **2018**, *9*, 1687.
21. Cai, J.; Ruffieux, P.; Jaafar, R.; Bieri, M.; Braun, T.; Blankenburg, S.; Muoth, M.; Seitsonen, A. P.; Saleh, M.; Feng, X.; Müllen, K.; Fasel, R. Atomically precise bottom-up fabrication of graphene nanoribbons. *Nature* **2010**, *466*, 470-473.
22. Talirz, L.; Ruffieux, P.; Fasel, R. On-surface synthesis of atomically precise graphene nanoribbons. *Adv. Mater.* **2016**, *28*, 6222-6231.
23. Liu, Z.; Fu, S.; Liu, X.; Narita, A.; Samorì, P.; Bonn, M.; Wang, H. I. Small Size, Big Impact: Recent Progress in Bottom-Up Synthesized Nanographenes for Optoelectronic and Energy Applications. *Adv. Sci.* **2022**, *9*, 2106055.
24. Bronner, C.; Stremlau, S.; Gille, M.; Brauße, F.; Haase, A.; Hecht, S.; Tegeder, P. Aligning the band gap of graphene nanoribbons by monomer doping. *Angew. Chem. Int. Ed.* **2013**, *52*, 4422-4425.
25. Narita, A.; Feng, X.; Müllen, K. Bottom-up synthesis of chemically precise graphene nanoribbons. *Chem. Rec.* **2015**, *15*, 295-309.
26. Chen, Y.-C.; De Oteyza, D. G.; Pedramrazi, Z.; Chen, C.; Fischer, F. R.; Crommie, M. F. Tuning the band gap of graphene nanoribbons synthesized from molecular precursors. *ACS nano* **2013**, *7*, 6123-6128.
27. Wang, S.; Kharche, N.; Costa Girão, E.; Feng, X.; Müllen, K.; Meunier, V.; Fasel, R.; Ruffieux, P. Quantum dots in graphene nanoribbons. *Nano Lett.* **2017**, *17*, 4277-4283.
28. Borin Barin, G.; Sun, Q.; Di Giovannantonio, M.; Du, C. Z.; Wang, X. Y.; Llinas, J. P.; Mutlu, Z.; Lin, Y.; Wilhelm, J.; Overbeck, J.; Daniels, C.; Lamparski, M.; Sahabudeen, H.; Perrin, M. L.; Urgel, J. I.; Mishra, S.; Kinikar, A.; Widmer, R.; Stolz, S.; Bommert, M.; Pignedoli, C.; Feng, X.; Calame, M.; Müllen, K.; Narita, A.; Meunier, V.; Bokor, J.; Fasel, R.; Ruffieux, P. Growth Optimization and Device Integration of Narrow-Bandgap Graphene Nanoribbons. *Small* **2022**, *18*, 2202301.
29. Mehdi Pour, M.; Lashkov, A.; Radocea, A.; Liu, X.; Sun, T.; Lipatov, A.; Korlacki, R. A.; Shekhirev, M.; Aluru, N. R.; Lyding, J. W.; Sysoev, V.; Sinitskii, A. Laterally extended atomically precise graphene nanoribbons with improved electrical conductivity for efficient gas sensing. *Nat. Commun.* **2017**, *8*, 820.
30. Sainz, R.; Del Pozo, M.; Vázquez, L.; Vilas-Varela, M.; Castro-Esteban, J.; Blanco, E.; Petit-Domínguez, M. D.; Quintana, C.; Casero, E. Lactate biosensing based on covalent immobilization of lactate oxidase onto chevron-like graphene nanoribbons via diazotization-coupling reaction. *Anal. Chim. Acta* **2022**, *1208*, 339851.
31. Kosynkin, D. V.; Lu, W.; Sinitskii, A.; Pera, G.; Sun, Z.; Tour, J. M. Highly conductive graphene nanoribbons by longitudinal splitting of carbon nanotubes using potassium vapor. *ACS Nano* **2011**, *5*, 968-974.
32. Kimouche, A.; Ervasti, M. M.; Drost, R.; Halonen, S.; Harju, A.; Joensuu, P. M.; Sainio, J.; Liljeroth, P. Ultra-narrow metallic armchair graphene nanoribbons. *Nat. Commun.* **2015**, *6*, 10177.
33. Merino-Díez, N.; Garcia-Lekue, A.; Carbonell-Sanromà, E.; Li, J.; Corso, M.; Colazzo, L.; Sedona, F.; Sánchez-Portal, D.; Pascual, J. I.; de Oteyza, D. G. Width-dependent band gap in armchair graphene nanoribbons reveals Fermi level pinning on Au (111). *ACS Nano* **2017**, *11*, 11661-11668.
34. Jänsch, D.; Ivanov, I.; Zagranyarski, Y.; Duznovic, I.; Baumgarten, M.; Turchinovich, D.; Li, C.; Bonn, M.; Müllen, K. Ultra-Narrow Low-Bandgap Graphene Nanoribbons from Bromoperylenes—Synthesis and Terahertz-Spectroscopy. *Chem. Eur. J.* **2017**, *23*, 4870-4875.
35. Yang, W.; Lucotti, A.; Tommasini, M.; Chalifoux, W. A. Bottom-up synthesis of soluble and narrow graphene nanoribbons using alkyne benzannulations. *J. Am. Chem. Soc.* **2016**, *138*, 9137-9144.
36. Jordan, R. S.; Li, Y. L.; Lin, C.-W.; McCurdy, R. D.; Lin, J. B.; Brosmer, J. L.; Marsh, K. L.; Khan, S. I.; Houk, K.; Kaner, R. B.; Rubin, Y. Synthesis of *N* = 8 armchair graphene nanoribbons from four distinct polydiacetylenes. *J. Am. Chem. Soc.* **2017**, *139*, 15878-15890.

37. Yamaguchi, J.; Hayashi, H.; Jippo, H.; Shiotari, A.; Ohtomo, M.; Sakakura, M.; Hieda, N.; Aratani, N.; Ohfuchi, M.; Sugimoto, Y.; Yamada, H.; Sato, S. Small bandgap in atomically precise 17-atom-wide armchair-edged graphene nanoribbons. *Commun. Mater.* **2020**, *1*, 36.
38. Lee, J.; Ryu, H.; Park, S.; Cho, M.; Choi, T.-L. Living Suzuki–Miyaura Catalyst-Transfer Polymerization for Precision Synthesis of Length-Controlled Armchair Graphene Nanoribbons and Their Block Copolymers. *J. Am. Chem. Soc.* **2023**, *145*, 15488-15495.
39. Wang, S.; Kharche, N.; Costa Girão, E.; Feng, X.; Müllen, K.; Meunier, V.; Fasel, R.; Ruffieux, P. Quantum dots in graphene nanoribbons. *Nano Lett.* **2017**, *17*, 4277-4283.
40. Takahashi, A.; Lin, C.-J.; Ohshimizu, K.; Higashihara, T.; Chen, W.-C.; Ueda, M. Synthesis and characterization of novel polythiophenes with graphene-like structures via intramolecular oxidative coupling. *Polym. Chem.* **2012**, *3*, 479-485.
41. Yao, X.; Zhang, H.; Kong, F.; Hinaut, A.; Pawlak, R.; Okuno, M.; Graf, R.; Horton, P. N.; Coles, S. J.; Meyer, E.; Bogani, L.; Bonn, M.; Wang, H. I.; Müllen, K.; Narita, A. N= 8 Armchair Graphene Nanoribbons: Solution Synthesis and High Charge Carrier Mobility. *Angew. Chem. Int. Ed.* **2023**, e202312610.
42. Chen, Z.; Wang, H. I.; Bilbao, N.; Teyssandier, J.; Prechtl, T.; Cavani, N.; Tries, A.; Biagi, R.; De Renzi, V.; Feng, X.; Kläui, M.; De Feyter, S.; Bonn, M.; Narita, A.; Müllen, K. Lateral fusion of chemical vapor deposited N= 5 armchair graphene nanoribbons. *J. Am. Chem. Soc.* **2017**, *139*, 9483-9486.
43. Sun, K.; Li, X.; Chen, L.; Zhang, H.; Chi, L. Substrate-controlled synthesis of 5-armchair graphene nanoribbons. *J. Phys. Chem. C* **2020**, *124*, 11422-11427.
44. Liu, Z.; Chen, Z.; Wang, C.; Wang, H. I.; Wuttke, M.; Wang, X.-Y.; Bonn, M.; Chi, L.; Narita, A.; Müllen, K. Bottom-up, on-surface-synthesized armchair graphene nanoribbons for ultra-high-power micro-supercapacitors. *J. Am. Chem. Soc.* **2020**, *142*, 17881-17886.
45. Li, G.; Yoon, K. Y.; Zhong, X.; Zhu, X.; Dong, G. Efficient bottom-up preparation of graphene nanoribbons by mild Suzuki–Miyaura polymerization of simple triaryl monomers. *Chem. Eur. J.* **2016**, *22*, 9116-9120.
46. Skraba-Joiner, S. L.; McLaughlin, E. C.; Ajaz, A.; Thamatam, R.; Johnson, R. P. Scholl cyclizations of aryl naphthalenes: rearrangement precedes cyclization. *J. Org. Chem.* **2015**, *80*, 9578-9583.
47. Note that in this five-membered intermediate, both aryl groups can undergo 1,2-migration. The lack of observation of the desired G0' product is likely due to its lower stability caused by steric repulsion between the two butyl substituents.
48. Schwab, M. G.; Narita, A.; Hernandez, Y.; Balandina, T.; Mali, K. S.; De Feyter, S.; Feng, X.; Müllen, K. Structurally defined graphene nanoribbons with high lateral extension. *J. Am. Chem. Soc.* **2012**, *134*, 18169-18172.
49. Centrone, A.; Brambilla, L.; Renouard, T.; Gherghel, L.; Mathis, C.; Müllen, K.; Zerbi, G. Structure of new carbonaceous materials: the role of vibrational spectroscopy. *Carbon* **2005**, *43*, 1593-1609.
50. Vo, T. H.; Shekhirev, M.; Lipatov, A.; Korlacki, R. A.; Sinitskii, A. Bulk properties of solution-synthesized chevron-like graphene nanoribbons. *Faraday Discuss.* **2014**, *173*, 105-113.
51. Malard, L. M.; Pimenta, M. A.; Dresselhaus, G.; Dresselhaus, M. S. Raman spectroscopy in graphene. *Phys. Rep.* **2009**, *473*, 51-87.
52. Ferrari, A. C.; Basko, D. M. Raman spectroscopy as a versatile tool for studying the properties of graphene. *Nat. Nanotechnol.* **2013**, *8*, 235-246.
53. Verzhbitskiy, I. A.; Corato, M. D.; Ruini, A.; Molinari, E.; Narita, A.; Hu, Y.; Schwab, M. G.; Bruna, M.; Yoon, D.; Milana, S.; Feng, X.; Müllen, K.; Ferrari, A. C.; Casiraghi, C.; Prezzi, D. Raman fingerprints of atomically precise graphene nanoribbons. *Nano Lett.* **2016**, *16*, 3442-3447.
54. Overbeck, J.; Barin, G. B.; Daniels, C.; Perrin, M. L.; Braun, O.; Sun, Q.; Darawish, R.; De Luca, M.; Wang, X.-Y.; Dumslaff, T.; Narita, A.; Müllen, K.; Ruffieux, P.; Meunier, V.; Fasel, R.; Calame, M. A universal length-dependent vibrational mode in graphene nanoribbons. *ACS Nano* **2019**, *13*, 13083-13091.

55. Chen, Z.; Wang, H. I.; Teyssandier, J.; Mali, K. S.; Dumslaff, T.; Ivanov, I.; Zhang, W.; Ruffieux, P.; Fasel, R.; Räder, H. J.; Turchinovich, D.; De Feyter, S.; Feng, X.; Kläui, M.; Narita, A.; Bonn, M.; Müllen, K. Chemical vapor deposition synthesis and terahertz photoconductivity of low-band-gap *N* = 9 armchair graphene nanoribbons. *J. Am. Chem. Soc.* **2017**, *139*, 3635-3638.
56. Borin Barin, G.; Fairbrother, A.; Rotach, L.; Bayle, M.; Paillet, M.; Liang, L.; Meunier, V.; Hauert, R.; Dumslaff, T.; Narita, A.; Müllen, K.; Sahabudeen, H.; Berger, R.; Feng, X.; Fasel, R.; Ruffieux, P. Surface-synthesized graphene nanoribbons for room temperature switching devices: substrate transfer and *ex situ* characterization. *ACS Appl. Nano Mater.* **2019**, *2*, 2184-2192.
57. Makuła, P.; Pacia, M.; Macyk, W. How to correctly determine the band gap energy of modified semiconductor photocatalysts based on UV–Vis spectra. *J. Phys. Chem. Lett.* **2018**, *9*, 6814-6817.
58. Sakaguchi, H.; Kawagoe, Y.; Hirano, Y.; Iruka, T.; Yano, M.; Nakae, T. Width-Controlled Sub-Nanometer Graphene Nanoribbon Films Synthesized by Radical-Polymerized Chemical Vapor Deposition. *Adv. Mater.* **2014**, *26*, 4134-4138.
59. Brixner, T.; Hildner, R.; Köhler, J.; Lambert, C.; Würthner, F. Exciton transport in molecular aggregates–from natural antennas to synthetic chromophore systems. *Adv. Energy Mater.* **2017**, *7*, 1700236.
60. Albrecht, P.; Lyding, J. Ultrahigh-vacuum scanning tunneling microscopy and spectroscopy of single-walled carbon nanotubes on hydrogen-passivated Si (100) surfaces. *Appl. Phys. Lett.* **2003**, *83*, 5029-5031.
61. Radocea, A.; Sun, T.; Vo, T. H.; Sinitskii, A.; Aluru, N. R.; Lyding, J. W. Solution-synthesized chevron graphene nanoribbons exfoliated onto H: Si (100). *Nano Lett.* **2017**, *17*, 170-178.
62. Celis, A.; Nair, M. N.; Taleb-Ibrahimi, A.; Conrad, E. H.; Berger, C.; De Heer, W.; Tejeda, A. Graphene nanoribbons: fabrication, properties and devices. *J. Phys. D: Appl. Phys.* **2016**, *49*, 143001.
63. Xu, Y.; He, K.; Schmucker, S.; Guo, Z.; Koepke, J.; Wood, J.; Lyding, J.; Aluru, N. Inducing electronic changes in graphene through silicon (100) substrate modification. *Nano Lett.* **2011**, *11*, 2735-2742.
64. Denk, R.; Hohage, M.; Zeppenfeld, P.; Cai, J.; Pignedoli, C. A.; Söde, H.; Fasel, R.; Feng, X.; Müllen, K.; Wang, S.; Prezzi, D.; Ferretti, A.; Ruini, A.; Molinari, E.; Ruffieux, P. Exciton-dominated optical response of ultra-narrow graphene nanoribbons. *Nat. Commun.* **2014**, *5*, 4253.
65. Talirz, L.; Söde, H.; Dumslaff, T.; Wang, S.; Sanchez-Valencia, J. R.; Liu, J.; Shinde, P.; Pignedoli, C. A.; Liang, L.; Meunier, V.; Plumb, N. C.; Shi, M.; Feng, X.; Narita, A.; Müllen, K.; Fasel, R.; Ruffieux, P. On-surface synthesis and characterization of 9-atom wide armchair graphene nanoribbons. *ACS Nano* **2017**, *11*, 1380-1388.
66. Liu, X.; Li, G.; Lipatov, A.; Sun, T.; Mehdi Pour, M.; Aluru, N. R.; Lyding, J. W.; Sinitskii, A. Chevron-type graphene nanoribbons with a reduced energy band gap: Solution synthesis, scanning tunneling microscopy and electrical characterization. *Nano Res.* **2020**, *13*, 1713-1722.
67. Nguyen, G. D.; Tsai, H.-Z.; Omrani, A. A.; Marangoni, T.; Wu, M.; Rizzo, D. J.; Rodgers, G. F.; Cloke, R. R.; Durr, R. A.; Sakai, Y.; Liou, F.; Aikawa, A. S.; Chelikowsky, J. R.; Louie, S. G.; Fisher, F. R.; Crommie, M. F. Atomically precise graphene nanoribbon heterojunctions from a single molecular precursor. *Nat. Nanotechnol.* **2017**, *12*, 1077-1082.
68. Llinas, J. P.; Fairbrother, A.; Borin Barin, G.; Shi, W.; Lee, K.; Wu, S.; Yong Choi, B.; Braganza, R.; Lear, J.; Kau, N.; Choi, W.; Chen, C.; Pedramrazi, Z.; Dumslaff, T.; Narita, A.; Feng, X.; Müllen, K.; Fischer, F.; Zettl, A.; Ruffieux, P.; Yablonovitch, E.; Crommie, M.; Fasel, R.; Bokor, J. Short-channel field-effect transistors with 9-atom and 13-atom wide graphene nanoribbons. *Nat. Commun.* **2017**, *8*, 633.
69. Shekhirev, M.; Lipatov, A.; Torres, A.; Vorobeva, N. S.; Harkleroad, A.; Lashkov, A.; Sysoev, V.; Sinitskii, A. Highly selective gas sensors based on graphene nanoribbons grown by chemical vapor deposition. *ACS Appl. Mater. Interfaces* **2020**, *12*, 7392-7402.
70. Shekhirev, M.; Vo, T. H.; Mehdi Pour, M.; Lipatov, A.; Munukutla, S.; Lyding, J. W.; Sinitskii, A. Interfacial self-assembly of atomically precise graphene nanoribbons into uniform thin films for electronics applications. *ACS Appl. Mater. Interfaces* **2017**, *9*, 693-700.

71. Lipatov, A.; Varezhnikov, A.; Augustin, M.; Bruns, M.; Sommer, M.; Sysoev, V.; Kolmakov, A.; Sinitskii, A. Intrinsic device-to-device variation in graphene field-effect transistors on a Si/SiO2 substrate as a platform for discriminative gas sensing. *Appl. Phys. Lett.* **2014**, *104*, 013114.
72. Lipatov, A.; Varezhnikov, A.; Wilson, P.; Sysoev, V.; Kolmakov, A.; Sinitskii, A. Highly selective gas sensor arrays based on thermally reduced graphene oxide. *Nanoscale* **2013**, *5*, 5426-5434.
73. Lipatov, A.; Guinel, M. J.-F.; Muratov, D. S.; Vanyushin, V. O.; Wilson, P. M.; Kolmakov, A.; Sinitskii, A. Low-temperature thermal reduction of graphene oxide: In situ correlative structural, thermal desorption, and electrical transport measurements. *Appl. Phys. Lett.* **2018**, *112*, 053103.
74. Pazniak, H.; Plugin, I. A.; Loes, M. J.; Inerbaev, T. M.; Burmistrov, I. N.; Gorshenkov, M.; Polcak, J.; Varezhnikov, A. S.; Sommer, M.; Kuznetsov, D. V.; Bruns, M.; Fedorov, F. S.; Vorobeva, N. S.; Sinitskii, A.; Sysoev, V. V. Partially oxidized $Ti_3C_2T_x$ MXenes for fast and selective detection of organic vapors at part-per-million concentrations. *ACS Appl. Nano Mater.* **2020**, *3*, 3195-3204.
75. Loes, M. J.; Bagheri, S.; Vorobeva, N. S.; Abourahma, J.; Sinitskii, A. Synergistic Effect of TiS_3 and $Ti_3C_2T_x$ MXene for Temperature-Tunable p-/n-Type Gas Sensing. *ACS Appl. Nano Mater.* **2023**, *6*, 9226-9235.